INSTITUTE FOR FUSION STUDIES

DOE/ET-53088-555 IFSR #555

Explicit, Analytical and Numerical Solution of the Nonlinear Vlasov Poisson System

V. ŠKARKA
International Centre for Theoretical Physics
Trieste, Italy
S.M. MAHAJAN
IFS-UT-Austin
Austin, Texas 78712
E. FIJALKOW
Phisique, Mathematique
Modelisation et Simulation, C.N.R.S.
Orleans, France

June 1992

THE UNIVERSITY OF TEXAS

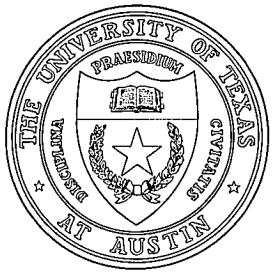

AUSTIN

Explicit, Analytical and Numerical Solution of the Nonlinear Vlasov Poisson System

V. Škarka, S.M. Mahajan[a)]
International Centre for Theoretical Physics
Trieste, Italy
and
E. Fijalkow
Phisique, Mathematique
Modelisation et Simulation, C.N.R.S.
Orleans, France

Abstract

In order to describe the time evolution of an inhomogeneous collisionless plasma the nonlinear Vlasov equation is solved perturbatively, using subdynamics approach and the diagrammatic techniques. The solution is given in terms of a double perturbation series, one with respect to the nonlinearities and other with respect to the interaction between particles. The infinite sum of interaction terms can be performed exactly due to the property of dynamical factorization. Following the methodology, the exact solution in each order with respect to nonlinearities is computed. For a choice of initial perturbation the first order exact solution is numerically integrated in order to find the local density excess. The approximate analytical solution is found to be in excellent agreement with exact numerical results. Analytical computation gives a better insight into the problem and it has the advantage to be simpler, and also accessible in some range of parameters where it is difficult to find numerical solutions.

[a)]Institute for Fusion Studies, The University of Texas at Austin, Austin, Texas 78712

I. Introduction

The time evolution of a quasi electrostatic plasma in the regime where the collisions are negligible is governed by a pair of coupled equations; Poisson equation for electric potential and the "collisionless" Boltzmann equation, i.e. the Liouville equation for one particle distribution function. By requiring that the electric field in the Liouville equation be self-consistently generated by the motion of electrons, this set of coupled equations can be reduced to the Vlasov equation. Being nonlinear, such an equation is hard to solve. A considerable effort has been invested over many years in seeking its solutions numerically (using either Eulerian or particle codes) [1-3] as well as analytically [4-7]. Montgomery formally extended Landau's method to the nonlinear case, but offered no proof of completeness and gave no explicit computations [8]. A somewhat different approach, using the subdynamics methodology established by the Brussels Group, seems to offer interesting possibilities [9].

The concept of subdynamics was introduced by Prigogine, George, and Henin [10], and was further elaborated by Balescu [11, 12] in order to derive kinetic equations. Following this method, the dynamics of a large system is split into a complete set of independent subdynamics [13]. Using the resolvent formalism, this approach has been recently extended to inhomogeneous gases and plasmas [14]. The method was also successfully used to obtain formal solution of the nonlinear Vlasov equation, where it represents a generalization of Van Kampen and Case's treatment of the linearized equation [15-18]. The subdynamics approach has been later on generalized to deal with plasmas open to interaction with time-dependent external fields [19, 20].

In the present paper, the general analytical solution of the nonlinear Vlasov equation is explicitly computed and expressions for space-time variation of the local density excess for different initial conditions are derived.

II. General Formalism

We begin by a short review of the subdynamics formalism developed primarily to deal with problems in nonequilibrium statistical mechanics. In this approach the plasma is considered not as a fluid but as a one-component gas of charged particles (e is the charge) moving in a neutralizing background, and interacting through the Coulomb potential [12]

$$e^2 V_{jn} = \frac{e^2}{|x_j - x_n|} \,. \tag{1}$$

The dynamics of such a large system is governed by the Liouville equation for the N-particle distribution function

$$i \frac{\partial \rho(\mathbf{q}, \mathbf{v}; t)}{\partial t} = L\rho(\mathbf{q}, v; t) \,. \tag{2}$$

The Liouvillian L is split into a free part

$$L_0 = -i \sum_{j=1}^{N} \mathbf{v}_j \cdot \frac{\partial}{\partial \mathbf{q}_j} \tag{3}$$

and a part which represents the interaction (m is the particle mass),

$$e^2 L_1 = ie^2 \sum_{j<n} \sum \frac{1}{m} \frac{\partial V_{jn}}{\partial \mathbf{q}_j} \left(\frac{\partial}{\partial \mathbf{v}_j} - \frac{\partial}{\partial \mathbf{v}_n} \right) \,. \tag{4}$$

Equations (2)–(4) constitute an essentially exact description of the plasma as a collection of charged particles, each interacting simultaneously with a large number of others. Taking advantage of its linearity, the Liouville equation can be formally solved as

$$\rho(\mathbf{q}, \mathbf{v}; t) = \frac{1}{2\pi i} \int_c dz \, e^{-izt} \frac{1}{z - L_0 - e^2 L_1} \rho(\mathbf{q}, \mathbf{v}; 0) \,. \tag{5}$$

The resolvent of the total Liouvillian is then expanded with respect to the interaction

$$\frac{1}{z - L_0 - e^2 L_1} = \sum_{n=0}^{\infty} \frac{1}{z - L_0} \left(e^2 L_1 \frac{1}{z - L_0} \right)^n \tag{6}$$

which, along with the Fourier expansion of the distribution function (Ω is the volume)

$$\rho(\mathbf{q}, \mathbf{v}; t) = \frac{1}{\Omega^N} \sum_{\mathbf{k}_1} \cdots \sum_{\mathbf{k}_N} \rho_{(\mathbf{k}_1, \ldots, \mathbf{k}_N)}(\mathbf{v}_1, \ldots, \mathbf{v}_N; t) e^{i \sum_{n=1}^{N} \mathbf{k}_n \cdot \mathbf{q}_n} \tag{7}$$

allows us to write the formal solution in the representation of the eigenfunctions of the unperturbed Liouvillian, L [14]

$$\rho_{\{\mathrm{k}\}}(\mathrm{v};t) = \frac{1}{2\pi i}\int_c dz\, e^{-izt} \sum_{\{\mathrm{k}'\}} \sum_{n=0}^{\infty} \left\langle \{\mathrm{k}\} \left| \frac{1}{z-L_0} \left[e^2 L_1 \frac{1}{z-L_0} \right]^n \right| \{\mathrm{k}'\} \right\rangle \rho_{\{\mathrm{k}'\}}(\mathrm{v},0)\,. \qquad (8)$$

The Fourier components, in general, have simple physical interpretations in terms of inhomogeneities and correlations between various degrees of freedom. The correlations and the inhomogeneities are associated with the wave vectors in the Fourier coefficients $\rho_{\{\mathrm{k}\}}$ and in the unperturbed resolvent, i.e. in the free propagators:

$$\left\langle \{\mathrm{k}\} \left| \frac{1}{z-L_0} \right| \{\mathrm{k}'\} \right\rangle = \frac{1}{z - \sum_{j=1}^{N} \mathrm{k}_j \cdot \mathrm{v}_j} \prod_{j=1}^{N} \delta_{-\mathrm{k}'_j;\mathrm{k}_j}\,. \qquad (9)$$

The system evolves because of the change in correlations caused by the binary interactions; in all these interactions, the total wave vector $\mathbf{K} = \sum_n \mathrm{k}_n$ is conserved:

$$\left\langle \{\mathrm{k}\} \left| e^2 L_1 \right| \{\mathrm{k}'\} \right\rangle = \sum_{j<n} \sum_{\ell} \frac{8\pi^3}{\Omega m} V_\ell \boldsymbol{\ell} \left(\frac{\partial}{\partial \mathrm{v}_j} - \frac{\partial}{\partial \mathrm{v}_n} \right) \delta_{\mathrm{k}'_j + \boldsymbol{\ell} - \mathrm{k}_j} \delta_{\mathrm{k}'_n - \boldsymbol{\ell} - \mathrm{k}_n} \prod_{a(\neq j,n)} \delta_{-\mathrm{k}'_a,\mathrm{k}_a}\,. \qquad (10)$$

In Eq. (10), $V_{\boldsymbol{\ell}}$'s are the coefficients in the Fourier expansion of the interaction potential. In an inhomogeneous plasma, the total wave vector $\mathbf{K}$ must be different from zero; the inhomogeneous vacuum of correlations is defined by the set of Fourier coefficients, $\rho_{0,\ldots,\mathbf{K}_\alpha,\ldots,0}(\mathbf{v}_j;t)$ with only one non zero wave vector $\mathbf{K}_\alpha = \mathbf{K}$. Such a dynamics of correlations admits a very useful diagrammatic representation, in which for instance, the propagator of the $\mathbf{K}$-inhomogeneous vacuum of correlations is drawn as one line [14]. The correlations are classified with respect to the minimum number of interactions needed to create them from the $\mathbf{K}$-vacuum. Each interaction (10) changes the correlations, and is represented by an elementary vertex (Fig. 1) [12]. Using these elementary vertices, a diagram can be associated by one to one correspondence to each transition in (8).

The next step is to compute the residues at various poles of the expanded resolvent (7). Only the residue at the pole η contributes to the (η) subdynamics. The pole η of a propagator,

being a particular eigenvalue of the unperturbed Liouvillian $\langle\eta|L_0|\eta\rangle$, is associated with a correlation η given by the corresponding set of wave vectors. Therefore, there are as many subdynamics as there are correlations and the distribution function $\rho_\nu(\mathbf{v};t)$ can be decomposed in terms of components $\rho_\nu^{(\eta)}(\mathbf{v};t)$ contributing to various subdynamics (η):

$$\rho_\nu(\mathbf{v};t) = \sum_\eta \rho_\nu^{(\eta)}(\mathbf{v};t) \; . \tag{11}$$

The essence of this approach lies in the fact that each (η) subdynamics evolves independently. If this were not the case, the breakdown into various subdynamics will not be particularly useful or even meaningful. The evolution equation is of the form

$$\frac{\partial}{\partial t}\,\rho_\nu^{(\eta)}(t) = -i\mathcal{C}_{\nu\eta}\left\{\langle\eta|L_0|\eta\rangle + \Theta_\eta\right\}\rho_\eta^{(\eta)}(t) \; , \tag{12}$$

and is obtained from the formally exact solution [14] [constructed from (8)]:

$$\begin{aligned}\rho_\nu^{(\eta)}(\mathbf{v};t) &= \mathcal{C}_{\nu\eta}\, e^{-it\{\langle\eta|L_0|\eta\rangle+\Theta_\eta\}}\mathcal{A}_\eta \sum_\mu \mathbb{D}_{\eta\mu}\,\rho_\mu(\mathbf{v};0) \\ &= \mathcal{C}_{\nu\eta}\, e^{-it\{\langle\eta|L_0|\eta\rangle+\Theta_\eta\}}\mathcal{A}_\eta\,\rho_\eta^{(\eta)}(\mathbf{v};0)\end{aligned} \tag{13}$$

by collecting together the contributions from the residue of the same pole (η). In the expression (13) $\mathcal{C}_{\nu\eta}$ stands for the creation superoperator. The distribution function $\rho_\eta^{(\eta)}(v;0)$ includes the destruction superoperator $\mathbb{D}_{\eta\mu}$ and it defines the "postinitial conditions." The superoperators $\mathcal{C}_{\nu\eta}$ and $\mathbb{D}_{\eta\mu}$ correspond to the off-diagonal contributions. The collision superoperator Θ_η to which $\mathcal{A}_\eta$ is functionally related, comes from the diagonal transitions.

III. Solution of the Vlasov Equation

Following Balescu, we now simplify Eq. (12)–(13) in the Vlasov approximation [12]. With the collision superoperator $\Theta_\eta = 0$, one obtains, from the formalism of Sec. 2, the Vlasov equation in Fourier representation

$$\frac{\partial}{\partial t}\,\rho_K(v_a;t) + iKv\rho_K(v_a;t) = i\,\frac{\omega_p^2}{K^2}\,\frac{\partial\varphi(v_a;t)}{\partial v_a}\int_{-\infty}^{\infty} dv_j\,\rho_K(v_j;t)$$

$$+\frac{\partial}{\partial v_a}\int_{-\infty}^{\infty} dv_j\,\frac{\omega_p^2\ell}{\ell^2}\,\varphi_{(K-\ell)}(v_a;t)\varphi_\ell(v_j;t) \tag{14}$$

along with a consistent scheme for constructing its perturbative solution [15]. The Vlasov equation (14) is obtained when the Poisson equation is solved and the electric potential (as a functional of the inhomogeneous one-particle distribution function $\varphi_K(v;t)$) is substituted into the Liouville equation, making the force term nonlinear. Notice that in Eq. (14), $\mathcal{A}(v_a;t)$ is the homogeneous one-particle distribution function and $\omega_p = (4\pi ne^2/m)^{1/2}$ is the plasma frequency depending on the number density n.

In the classical plasma approximation achieved at low densities or at high temperatures, the dimensionless parameter

$$g \sim \left(\frac{n^{\frac{1}{3}}e^2}{\kappa T}\right)^{\frac{3}{2}} \sim \frac{1}{n\lambda_D^3} \ll 1$$

is very small implying that the relaxation time $\tau_r = m^{1/2}/e^4 n(\kappa T)^{-\frac{3}{2}}$ can be very long, much longer than the plasma characteristic time which is proportional to the inverse of the plasma frequency ω_p. As a consequence, an expansion of the formal solution (13) in which only the terms proportional to powers of e^2n are retained, corresponds to the formal solution of the Vlasov equation [15]:

$$\begin{aligned} f_{K_a}(t) &= \sum_\eta f_{K_a}^{(\eta)}(t) = \sum_\eta \int_{-\infty}^{\infty} dv\, \mathcal{C}_{K_a;\eta}\, e^{-it\langle\eta|L_0|\eta\rangle} \sum_\mu \mathbb{D}_{\eta\mu} \prod_i f_{\mu_i}(0) \\ &= \sum_\eta \int_{-\infty}^{\infty} dv\, \mathcal{C}_{K_a;\eta}\, e^{-it\langle\eta|L_0|\eta\rangle} \prod_i f_{\eta_i}^{(\eta)}(0)\,. \end{aligned} \tag{15}$$

In terms of the diagram given in Fig. 1, C, D and E are the only elementary vertices proportional to e^2n. Since the solution is an inhomogeneous one-particle distribution function, the corresponding connected diagrams necessarily end with an external line at the left. If such a diagram is constructed using the elementary vertex C, it is always negligible in the thermodynamic limit (in which the number N of particles and the volume Ω containing

them, both tend to infinity in such a way that the density n remains finite) [21]. Therefore, the solution (15) contains all possible combinations of only two elementary vertices, D and E. Displayed in Fig. 2 [18], these vertices are conveniently referred to as the 'fork' and the 'loop' respectively. The dots between loops indicate all possible number of additional loops. For instance the first diagram {a} in Fig. 2 corresponds to the sum of the entire family of diagrams with number of loops ranging from one to infinity. Such an infinite series of diagrams with contributions proportional to powers of e^2n must be summed in order to get a physically consistent result. The first family of diagrams constitute the linear solution: the final one-particle distribution function is related to a single power of the initial one-particle function. All other diagrams connect, in a nonlinear way, the final distribution function with two or more initial one-particle distribution functions.

IV. Solution of the Linearized Vlasov Equation

The solution to the linearized Vlasov (Eq. (14) without the last term on the right-hand side) is fully given in terms of diagrams with loop vertices. The fork diagrams contribute only to the nonlinear part. The contribution of a typical one loop diagram to the solution of the linearized equation, written explicitly using expressions (8)–(10), is given as

$$f_K(v_a;t) = \frac{1}{2\pi i}\int_c dz\, e^{-izt}\frac{1}{z-Kv_a}\int_{-\infty}^{\infty} dv_j \frac{4\pi e^2 n}{m}\frac{K}{K^2}\frac{\partial\varphi(v_a;0)}{\partial v_a}\frac{1}{z-Kv_j} f_K(\mathbf{v}_j;0)\ . \quad (16)$$

Computing the residue corresponding to the pole K_jv_j of the initial propagator, we express the solution in terms of an experimentally measurable quantity, the local density excess $h(t)$.

$$h_K^{(K_j)}(t) = \int_{-\infty}^{\infty} dv_a f_K(v_a;t) = \int_{-\infty}^{\infty} dv_j \int_{-\infty}^{\infty} dv_a \frac{(-1)}{i\xi - K(v_a - v_j)}\frac{\omega_p^2 K}{K^2}\frac{\partial\varphi(v_a;0)}{\partial v_a}$$

$$\cdot\ e^{e^{-itKv_j}} f_K(v_j;0) \equiv \int_{-\infty}^{\infty} dv_j \mathcal{J} e^{-itKv_j} f_K(v_j;0)\ . \quad (17)$$

In this way, the contribution to the solution, associated with the pole K_jv_j (in the sub-dynamics (K_j)) is obtained. The infinitesimal imaginary part $i\xi$ appears in the propagator

through the analytic continuation procedure. The regularization recipe is called the $i\xi$-rule in the resolvent formalism; a small positive (negative) imaginary part $i\xi(\xi > 0)$ is added to the denominators of the propagators belonging to a state more (less) correlated than the one whose subdynamics is sought [22]. Each loop represents a binary interaction so that many loops correspond to the interaction between many particles. In the collisionless plasma each particle interacts simultaneously with a large number of other particles due to the long range Coulomb forces. Therefore, in order to describe the collective effects (such as screening) correctly, the higher order terms in the infinite series of the loop diagrams (Fig. 2.) cannot be dropped. The sum of all loops has to be computed. Fortunately, each new loop changes the name (label) of the particle so that the term corresponding to a loop commutes with all other loop terms. Consequently, the two-loops diagram contributes to the same subdynamics (K_j) the product of two $\mathcal{J}$ terms and so on. Therefore, the sum of the whole family of diagrams {a} in Fig. 2. corresponds to a geometrical progression whose exact sum $\{(1-J)^{-1}\}$ is inversely proportional to the dielectric function:

$$\varepsilon = 1 - \mathcal{J} = 1 - \int_{-\infty}^{\infty} dv_x \frac{\omega_p^2 K}{K^2} \frac{(-1)}{i\xi - K(v_x - v_y)} \frac{\partial \varphi(v_x;0)}{\partial v_x} \,. \tag{18}$$

The solution in the other subdynamics associated with other poles can be obtained in the same manner. The solution of linearized Vlasov equation corresponds to the sum over all subdynamics (K_j), i.e. to the sum over all possible particles j:

$$\begin{aligned} h_K(t) = \sum_j h_K^{(K_j)}(t) &= \int_{-\infty}^{\infty} dv_j \frac{1}{1-\mathcal{J}} e^{-itKv_j} f_K^{(K_j)}(0) \\ &= \int_{-\infty}^{\infty} dv_j \frac{e^{-itKv_j}}{\varepsilon} f_K^{(K_j)}(0) = \int_{-\infty}^{\infty} dv_j \, \mathcal{C}_{K_a;K_j} \, e^{-itKv_j} f_K^{(K_j)}(0) \,. \end{aligned} \tag{19}$$

In the last line the linearized solution is written in the from (15) and the destruction superoperator $\mathbb{D}$ is absorbed into the "postinitial" distribution function $f_K^{(K_j)}(0)$, so that only the creation superoperator $\mathcal{C}_{K_a;K_j}$ needs to be computed [18]. As a corollary, one need only to compute the subdynamics associated with the states present at the extreme right-hand

side of each diagram and when the sum over all diagrams is made, the contributions to all possible subdynamics are collected.

Notice that the solution in each subdynamics (K_j) describes the free propagation of an undamped plasma mode corresponding to the eigenvalue Kv_j, and is thus equivalent to the distribution obtained by van Kampen and Case [16,17]. Summation over all subdynamics (19) (a complete set) corresponds to the superposition of these plane-wave eigenfunctions, yielding the exact solution of the linearized equation. Since the subdynamics form a complete set (a suitable basis for decomposition), the current method is an appropriate nonlinear generalization of the van Kampen-Case treatment [18].

V. Nonlinear Solution

The solution of the nonlinear Vlasov equation (14) is represented in Fig. 1 by the family of diagrams {b}, {c}, etc. [18]. It is a double perturbation series, with respect to the interactions between the particles with the same wave vector (loop vertices) and with respect to the nonlinearity (fork vertices). The nonlinear contribution of fork diagrams have to be computed order by order. At each order, one has to perform the summation over the infinite series of interactions (loop vertices), in order to insure that the collective effects are correctly described.

Starting from Eq. (8), the contribution of family of diagrams in Fig. 2, as well as of those of higher order, has been already computed elsewhere [18]. The basic purpose of this paper is to find explicit analytical expressions for the physically relevant quantities. Limiting the calculation to the first order in nonlinearity, we find the local density excess to be

$$h_K(t) = \sum_\eta h_K^{(\eta)}(t) = \int_{-\infty}^{\infty} dv\, e^{-itKv} \frac{f_K(0)}{\varepsilon(K)} + \int_{-\infty}^{\infty} \prod_i dv_i \int_{-\infty}^{\infty} d\ell\, \frac{1}{\varepsilon^{cc}(K,\ell)}$$

$$\cdot \left(D + D \cdot E \frac{1}{\varepsilon(\ell)} \right) \frac{1}{\varepsilon(K-\ell)}\, e^{-it\{(K-\ell)v_e + \ell v_j\}} f_{(K-\ell)}^{(K-\ell,\ell)}(0)\, f_\ell^{(K-\ell,\ell)}(0)\,. \qquad (20)$$

In order to understand the structure of the nonlinear terms, let us take a closer look at the diagrams {b} and {c} (of Fig. 2.). Notice that the line leading to the final state in the diagrams {b} and {c} is equivalent to the one corresponding to the linearized solution, and consequently contributes the factor ε^{-1} in the expression (20). The same holds for the lower line of the fork, since its mathematical expression commutes with the one of the fork vertex. Therefore, in order to obtain the expression corresponding to the whole family of diagrams {b}, only the contribution of the fork vertex D (see Fig. 1.) has to be computed explicitly, taking into account Gauss' theorem as it has been already done in Ref. 18. In diagram {c}, there are loops on the upper line also. The fork vertex D (i.e. its contribution) commutes with all except the loop E on its immediate right, since they both share the same particle c. Due to the property of dynamical factorization [18,23,24], contribution of all other loops on the same line can be summed independently of those on the lower line. The exact solution (20) up to the first order in nonlinearities can be written more explicitly as

$$
\begin{aligned}
h_K(t) = \int_{-\infty}^{\infty} dv_e \Bigg\{ & \frac{e^{-itKv_e}}{1 - \int_{-\infty}^{\infty} dv \, \frac{\omega_p^2}{K^2} \frac{1}{i\xi + v - v_e} \frac{\partial}{\partial v} \varphi(v;0)} f_K(v_e;0) \\
& + \int_{-\infty}^{\infty} dv_j \int_{-\infty}^{\infty} d\ell \, \frac{1}{1 - \int_{-\infty}^{\infty} dv \, \frac{\omega_p^2}{K^2} \frac{1}{i\xi + v - v_e - \frac{\ell}{K}(v_j - v_e)} \frac{\partial}{\partial v} \varphi(v;0)} \Bigg[\frac{\omega_p^2 \ell K}{(-i\xi + v_j - v_e)^2 \ell^4} \\
& + \int_{-\infty}^{\infty} dv_c \, \frac{1}{i\xi + v_c - v_e - \frac{\ell}{K}(v_j - v_e)} \, \frac{\omega_p^4 \ell}{\ell^2 (K-\ell)^2 K} \, \frac{\partial}{\partial v_c} \, \frac{1}{-i\xi + v_c - v_e} \\
& \cdot \frac{\partial \varphi(v_c;0)}{\partial v_c} \, \frac{1}{1 - \int_{-\infty}^{\infty} dv \, \frac{\omega_p^2}{(K-\ell)^2} \frac{1}{-i\xi + v - v_e} \frac{\partial \varphi(v;0)}{\partial v}} \Bigg] e^{-it\{Kv_e + \ell(v_j - v_e)\}} \cdot \\
& \cdot \frac{1}{1 - \int_{-\infty}^{\infty} dv \, \frac{\omega_p^2}{\ell^2} \frac{1}{-i\xi + v - v_j} \frac{\partial \varphi(v;0)}{\partial v}} \Bigg\} f_{K-\ell}(v_e;0) f_K(v_j,0) \, . \qquad (21)
\end{aligned}
$$

It is obvious from Eq. (21) that the explicit expressions tend to become long and unwieldy, and their further evaluation will be rather tedious if one does not resort to some well defined

systematic procedure. One thus needs a methodology to write final expressions directly from the diagrams, knowing that the diagrams bear one-to-one correspondence to the initial expressions. Such a procedure for direct transcription was developed in Ref. 18. It should be noted that the final algebraic expressions obtained after computing the residues of different poles (separation into the subdynamics), can be written in the same general form. The correspondence between this general form and the diagram from which it originates, has been found. An algorithm how to fill the general form, using the labels of the particles and wave vectors coming from a particular diagram, has also been established. This algorithm allows us to immediately write the final expression once the diagram is drawn. Tedious computations are avoided, and it becomes possible (whenever needed) to extend the calculation to higher orders.

Equation (21) is the main theoretical result on which further computations of this paper are based. The expression can be evaluated using numerical methods whenever an appropriate "equilibrium," and the initial disturbances are specified; most realistic plasma problems will require us to resort to numerical techniques. However, to establish the workability of this scheme, we deal with an idealized problem which allows an analytical solution under some drastic assumptions. The analytical solutions are compared with the exact numerical solutions to demonstrate that approximate analytical techniques can prove to be very useful. In future, we expect to carry the analytical methods further (make the approximations less drastic) and add to the understanding of nonlinear solutions.

For our test problem, we choose to study the evolution of a homogeneous plasma after it has been perturbed by a beam like pulse with a periodic modulation in space. Initial homogeneous one-particle distribution function is taken to be the Maxwellian

$$\varphi(v;0) = \sqrt{\frac{b}{\pi}}\, e^{-bv^2} \tag{22}$$

where $b^{-1/2} = v_{\rm th}$ is the thermal velocity. The perturbation, i.e. the initial inhomogeneous

one-particle distribution function, is sinusoidally modulated in space. This perturbation corresponds, in velocity space, to a shifted Maxwellian (u is the flow, and $\lambda^{-1/2} = \sigma$ is the thermal spread).

$$f(q,v;0) = \frac{A}{2}\int_{-\infty}^{\infty} dK e^{iqK}\sqrt{\frac{\lambda}{\pi}}\, e^{-\lambda(u-v)^2}\left\{\delta(K-2a)+\delta(K+2a)\right\} = A\sqrt{\frac{\lambda}{\pi}}\, e^{-\lambda(u-v)^2}\cos 2aq\ . \tag{23}$$

In terms of the first derivative of the plasma dispersion function

$$Z'(x) = -2 - 2x\pi^{-1/2}\int_{-\infty}^{\infty}\frac{1}{v-x}\, e^{-v^2}\, dv\ , \tag{24}$$

and the redefined variables $\alpha = i\xi - v_c - \frac{\ell}{K}(v_c - v_j)$; $\beta = i\xi + v_c$, $\gamma = i\xi + v_j$ the inverse Fourier transform of the solution can be written more compactly. For the particular choice of the wave number vector $K = \pm 2a$, the parameter $\mu = 4\omega_p^2 b/K^2 = \omega_p^2 b/a^2$, and the solution becomes

$$\begin{aligned} h(q;t) \doteq \int_{-\infty}^{\infty} dK e^{iqK}\int_{-\infty}^{\infty} d\beta\sqrt{\frac{\lambda}{\pi}}\Bigg\{ & \frac{e^{-\lambda(\beta-u)^2 - itK\beta}}{1-\frac{\mu}{4}Z'(\beta\sqrt{b})}\,\frac{A}{2}\Big[\delta(K-2a)+\delta(K+2a)\Big] \\ & + \int_{-\infty}^{\infty} d\gamma\sqrt{\frac{\lambda}{\pi}}\,\frac{\mu}{1-\frac{\mu}{4}Z'(\alpha\sqrt{b})}\Bigg[\frac{K}{4(\alpha+\beta)^2 b\ell} - \int_{-\infty}^{\infty} dv_c\,\frac{\mu K^3}{\ell(K-\ell)^2\sqrt{\pi b}} \\ & \frac{\partial}{\partial\alpha}\,\frac{v_c}{v_c+\alpha}\,\frac{e^{-bv_c^2}}{v_c-\beta}\,\frac{1}{1-\mu Z'(\alpha\sqrt{b})}\Bigg]\frac{e^{-\lambda(\gamma-u)^2+itK\alpha}}{1-\mu Z'(\gamma\sqrt{b})} \\ & \cdot\ \frac{A^2}{4}\left[\delta(K-2a)\delta(\ell-a)+\delta(K+2a)\delta(\ell+a)\right]\Bigg\}\ . \end{aligned} \tag{25}$$

The kernel of the last integral in (25) can also be expressed in terms of the Z-function. Variable transformations $\alpha = i\xi - \frac{1}{2}(v_e + v_j) = \frac{x}{\sqrt{2\lambda}}$; $\beta = i\xi + v_c = \frac{y-x}{\sqrt{2\lambda}}$, and $\gamma = i\xi + v_j = \frac{x+y}{\sqrt{2\lambda}} + 4i\xi$ with $x = \alpha\sqrt{2\lambda}$, $y = (\alpha+\beta)\sqrt{2\lambda}$, and $dxdy = \lambda d\beta d\gamma$ and $v = \beta\sqrt{\lambda}$ in the linearized term, lead to

$$h(t) = h_L(t) + h_{NL}(t) = \frac{A}{\sqrt{\pi}}\int_{-\infty}^{\infty} dv\,\frac{\cos 2a\left(q - \frac{vt}{\sqrt{\lambda}}\right)}{1-\frac{\mu}{4}Z'\{Gv\sqrt{2}\}}\, e^{-v^2+2vu\sqrt{\lambda}-\lambda u^2}$$

$$+\frac{A^2\mu}{2\pi}\int_{-\infty}^{\infty}dx\int_{-\infty}^{\infty}dy\Bigg\{\frac{1}{2G^2y^2}-\mu\left[\frac{y-x}{Gy^2}\left(Z\{Gx\}+Z\{G(y-x)\}\right)+\frac{x}{y}Z'\{Gx\}\right]$$

$$\cdot\frac{1}{1-\mu Z'\{G(y-x)\}}\Bigg\}\frac{e^{-y^2-2u^2\lambda}}{1-\frac{\mu}{4}Z'\{Gx\}}\frac{\cos 2a\left(q+\frac{tx}{\sqrt{2\lambda}}\right)}{1-\mu Z'\{-G(x+y)\}}e^{-x^2-2\sqrt{2\lambda}x} \tag{26}$$

where $G=(b/2\lambda)^{1/2}$ is a measure of the relative width (thermal spread) of the two Gaussians.

Before making further approximations, it is important to cast Eq. (26) into a form more suitable for numerical and further analytical computations. The apparent problem for numerical integration, associated with the double pole in the propagator (y^{-2}) is resolved by making a partial integration. Using Plemelj formula, then, allows one to explicitly display the principal part and the pole contribution [24]. The final formula Eq. (A1) of Appendix A, still constitutes an exact solution of the Vlasov equation correct to the first order in nonlinearity.

Further analytic progress involves making simplifying approximations. For this paper, we make rather drastic approximations to obtain an easily interpretable and compact expression giving the spatial and the temporal behavior of the perturbation. Our primary motive is to develop confidence in our analytical methods before we investigate more complicated problems.

Let us consider a beam-like pulse (with narrow thermal spread) propagating in a moderate temperature plasma. The parameter

$$G=\sqrt{\frac{b}{2\lambda}}\ll 1 \tag{27}$$

for this case, the small argument expansion of the Z-function will be adequate. A straightforward calculation yields, in the leading order, very simple linear $h_L(q;t)$ and nonlinear $h_{NL}(q;t)$ solutions:

$$h(q;t)=h_L(q;t)+h_{NL}(q;t)=\frac{A}{2+\mu}e^{-\frac{t^2a^2}{\lambda}}\cos[2a(q-tu)]$$

$$+\frac{A^2}{(2+\mu)\left(\frac{1}{\mu}+2\right)^2}\left\{6-\frac{\pi}{G}-\frac{1+2\mu}{\mu G^2}\right\}e^{-\frac{t^2a^2}{2\lambda}}\cos[2a(q-tu)]\,. \tag{28}$$

The observant reader well notice that the linear part of our result appears to be rather unusual. When the perturbation amplitude A goes to zero, h_L also goes to zero, because the denominator $2 + \mu \neq 0$. Under the specified conditions of our problem, there indeed are no normal modes of the plasma; the system was designed to study the propagation of a finite amplitude pulse in a plasma. However, all the physics of electrostatic plasmas, including plasma waves and Landau damping, is there in Eq. (26). In Appendix B, we explicitly show that with different approximations, we readily obtain Langmuir waves etc.

The analytical solution (28) will be now plotted as a function of space and time, in order to be compared with the "exact" solution obtained numerically. As usual in numerical computations, the parameters are rescaled; the plasma frequency ω_p, and the inverse square root of the width b are both taken to be unity. Choosing the amplitude of perturbation $A = 0.01$, together with the velocity shift $u = 0.2$, space and time behavior of the solution can be studied for different values of the wave vector a and the width parameter λ. For instance, for $a = 0.3$ and $\lambda = 10$, the superposition of the linearized and the nonlinear solutions is given in Fig. 3a. Such a perturbation, corresponding to a relatively wide Gaussian, is strongly damped due to the spread in velocity space and the interaction between particles.

In order to test the accuracy of the analytical results, the numerical methods of integration are applied to the solution (26). The linear part of solution is a one dimensional integral. The double integral of the nonlinear part is expressed in the more suitable form (A1) containing a single pole. The integral remains double only for the principal part of the propagator, while it reduces to the simple one for the pole contribution. The integrand is (in both parts) a functional of the dispersion function multiplied by Gaussians and a cosine with the argument increasing with time. When this argument is small, the integrand is a slowly varying function in time, and Gauss Hermite integration scheme with twenty points is used [25]. The integral is then exact for a polynomial of degree 41. For the growing argument of the cosine for larger times t, Filon's numerical integration is applied, since it is

well adapted to the rapidly varying functions [26]. A good approximation of the plasma dispersion function and its derivative is obtained by means of Padé approximation for Kummer function [27]. The accuracy of our program is tested by using Romberg integration. The 'exact' numerical solution corresponding to the parameters of Fig. 3a is plotted in Fig. 3b; the agreement is quite good.

For better visual comparison of the approximate analytical solution with the numerically integrated one, we shall superimpose the two solutions from now on. For $a = 0.3$ and $\lambda = 100$, Figs. 4 and 5 compare respectively the linear and the nonlinear parts of the solutions from the two approaches. The good agreement between the approximation and the "exact" solution is expected since the parameter $G = 0.07$ is comfortably small. Notice that the linearized solution is damped much quicker than the nonlinear one. The total excess density response, i.e., the sum of the linear and the nonlinear parts is displayed in Fig. 6 and shows good agreement as expected.

For the same $\lambda = 100$, we now vary the perturbation wave length; Figures 7 and 8correspond to $a = 0.5$ and 0.7 respectively. Increase of the wave vector a leads to quicker damping, and at the same time improves the agreement with the numerical solution.

Let us now make the perturbation more beam-like ($\lambda = 1000$) and at the same time also change the velocity shift $u = 0.1$ (see Fig. 10). The obtained approximate solution practically coincides with the exact one (parameter $G = 0.02$).

From Figs. 3, 7, and 9 ($a = 0.3$ for all of three), one notices that as the perturbation sharpens in velocity space, i.e. λ increases, the damping slows down. This behavior is predicted by Eq. (28), since the exponential decay time is $\tau_d \sim (\lambda/a^2)^{1/2}$.

Although the approximation used to obtain analytical solution is drastic, (even the Landau damping is thrown away), the agreement with the exact solution is excellent. This is because in investigated cases (where parameter G is very small) the disturbance is bodily carried away by the jet of incoming particles and the Landau damping is very small. This

damping will be dominant just in the opposite situations, when there is an appreciable fraction of injected particles having velocities larger than the thermal velocities of the medium, i.e. when the perturbation Gaussian is larger than the one of the medium: $G \gg 1$. This will be the subject of a forthcoming paper.

Accuracy of the analytical solution has also been successfully tested using Mathematica as a tool for numerical integration [28].

Having gained confidence in our approximation, which gets progressively better as G becomes small, we plot our analytic solution for $\lambda = 10000$, $a = 0.3$, and $u = 0.2$ (see Fig. 11). For such a large λ the numerical integration is no more possible. However, this case may be even more interesting (for an experimentalist) since it corresponds to the injection of an almost monoenergetic beam of particles into plasma. The obtained picture conforms to the fact that the more coherent the beam, the less is its spread in time. For the time interval for which the evolution of the system is followed (40 time units) the damping, due to the spread in velocity space, is inobservable.

VI. Conclusions

In this paper we have made use of the techniques of subdynamics formalism to obtain solutions of the nonlinear Vlasov equation. The subdynamics approach, developed for dealing with general many body systems, is clearly not the most efficient way for solving simple problems like the linear Vlasov-Poisson system. However, the formalism, with a little effort, can be marshalled to solve the nonlinear Vlasov equation for which few other means are available.

The diagrammatic techniques are particularly suited for doing higher order calculations. In this paper, however, we have limited ourselves to solving a rather idealized problem of the evolution of a sharp beam like pulse in an ambient plasma with moderate temperature. The explicit calculation is carried out to the leading order in the nonlinearity. Analytical and

numerical solutions are computed and are seen to be in very good agreement. This calculation is primarily meant to demonstrate the working of this methodology and, in particular, the excellent accuracy of our explicit analytical method. In future, we shall exploit this powerful technique to solve more and more involved problems in basic plasma physics. We would like to stress that the analytical methods used here can be extended to treat problems in higher spatial dimensions, where the numerical methods may be limited by the size of the actual computers.

Acknowledgments

We are grateful to Professor R. Balescu and Professor M. Feix, for helpful discussions. One of us (V. Š.) is indebted to Professor I. Prigogine for discussions and would like to thank Dr. A. Shiekh for stimulating suggestions and the help in implantation of Mathematica. Professor Abdus Salam, the International Atomic Energy Agency and UNESCO are gratefully acknowledged, for hospitality at the International Centre for Theoretical Physics, Trieste.

Appendix A

In order to facilitate the subsequent numerical and analytical computations, the double pole (y^{-2}) in the propagator of Eq. (26) is eliminated using partial integration. After some algebra, the remaining propagator (y^{-1}) is, by means of Plemelj formula, expressed in terms of the principal part and the pole contribution

$$h(q;t) = h_L(q;t) + h_{NL}(q;t) = \frac{A}{\sqrt{\pi}} \int_{-\infty}^{\infty} dv \, \frac{\cos 2a\left(q - \frac{vt}{\sqrt{\lambda}}\right)}{1 - \frac{\mu}{4} Z'\{Gv\sqrt{2}\}} \, e^{-v^2 + 2vu\sqrt{\lambda} - \lambda u^2}$$

$$+\frac{A^2\mu}{2} e^{-2\lambda u^2} \int_{-\infty}^{\infty} dx \, \frac{\cos 2a\left(q + \frac{tx}{\sqrt{2\lambda}}\right)}{1 - \frac{\mu}{4} Z'\{Gx\}} \, e^{-x^2 - 2\sqrt{2\lambda}x} \left\{ \frac{1}{\pi} \int_{-\infty}^{\infty} \frac{dy \, e^{-y^2}}{1 - \mu Z'\{-G(x+y)\}} \right.$$

$$\cdot \left[P \frac{\mu}{Gy} \left(\frac{z\{-G(x+y)\} - GxZ'\{-G(x+y)\}}{1 - \mu Z'\{-G(x+y)\}} + \frac{1}{1 - \mu Z'\{G(y-x)\}} \left[Gx(Z'\{G(y-x)\} - \right. \right. \right.$$

$$-Z'\{Gx\}) + (Z\{Gx\} + Z\{G(y-x)\}) \left\{ 2\mu Gx \left(\frac{Z\{-G(x+y)\} - GxZ'\{-G(x+y)\}}{1 - \mu Z'\{-G(x+y)\}} \right. \right.$$

$$\left. \left. \left. \left. - \frac{Z\{G(y-x) - GxZ'\{G(y-x)\}}{1 - \mu Z'\{-G(x+y)\}} \right) - 1 \right\} \right] \right) - \left(\frac{1}{G^2} + \frac{\mu Z'\{-G(x+y)\}}{1 - \mu Z'\{-G(x+y)\}} \right.$$

$$\left. + 2\mu x \left[\frac{1}{G} + \frac{\mu G Z'\{-G(x+y)\}}{1 - \mu Z'\{-G(x+y)\}} + \frac{\mu G Z'\{G(y-x)\}}{1 - \mu Z'\{G(y-x)\}} \right] \frac{Z\{Gx\} + Z\{G(y-x)\}}{1 - \mu Z'\{G(y-x)\}} \right) \Bigg]$$

$$\left. - \frac{i\mu(GxZ'\{Gx\} + Z\{Gx\})}{G(1 - \mu Z'\{-Gx\})^2} \right\} . \qquad \text{(A1)}$$

Appendix B

In this appendix we motivate the drastic approximations used to obtain Eq. (28) in which the linear term is a little unorthodox. To make contact with the usual plasma physics literature, we go back to the linear term of Eq. (21) (we could as well have used Eqs. (25)–(26))

$$h_K^L(t) = \int_{-\infty}^{\infty} \frac{dy\, e^{-itKy}\, f_K(y;0)}{1 - \int_{-\infty}^{\infty} dv\, \frac{\omega_p^2}{K^2} \frac{1}{v-y} \frac{\partial}{\partial v} \varphi(v,0)} \tag{B1}$$

where φ is the equilibrium distribution function and $f_K(y;0)$ is the initial disturbance. Let us take its Fourier transform

$$h_K^L(\omega) = \frac{1}{2\pi} \int_{-\infty}^{\infty} dt\, e^{i\omega t} h_K^L(t)\ . \tag{B2}$$

The integration over time yields the delta function $\delta(\omega - Ky)$ which allows y-integral to be trivially performed

$$h_K^L(\omega = \frac{f_K\left(\frac{\omega}{K};0\right)}{1 - \int_{-\infty}^{\infty} dv\, \frac{\omega_p^2}{K^2} \frac{1}{v-\omega/K} \frac{\partial}{\partial v} \varphi} = \frac{f_K\left(\frac{\omega}{K};0\right)}{\varepsilon(\omega,K)} \tag{B3}$$

which is the familiar expression. When $f_K \to 0, h_K^L(\omega)$, can remain finite, if $\varepsilon(\omega,K) = 0$ giving the standard normal mode; in this case the Langmuir wave. To derive the Langmuir wave, it is assumed that $\omega/K > v_{\text{th}}$ of the ambient plasma. For the idealized problem chosen in this section where $f_K \sim e^{-\lambda v^2}$ represents a sharp Gaussian compared to $\varphi \sim e^{-bv^2} (b/\lambda \ll 1)$, the situation is effectively reversed and the denominator reduces (in the leading order) to

$$\varepsilon(\omega,K) \simeq 1 - \frac{\omega_p^2}{K^2} \int \frac{\frac{\partial}{\partial v}\varphi}{v}\, dv = 1 + \frac{2b\omega_p^2}{K^2} \equiv 1 + \frac{\mu}{2} \tag{B4}$$

which contains no normal modes.

References

1. J.I. Schwarzmeier, H.R. Lewis, B. Abraham-Shrauner, and K.R. Symon, Phys. Fluids **22**, 1747 (1979).

2. A. Ghizzo, B. Izrar, P. Bertrand, E. Fijalkow, M.R. Feix and M. Shoucri, Phys. Fluids **31**, 72 (1988).

3. A. Ghizzo, P. Bertrand, M. Shoucri, T.W. Johnston, E. Fijalkow, M.R. Feix, J. Comput. Phys. **90**, 341 (1990).

4. T. Boutros-Ghali and T.H. Dupree Phys. Fluids **24**, 1839 (1981).

5. S.M. Mahajan, Phys. Fluids B **1**, 43 (1988).

6. R. Davidson, Methods in Nonlinear Plasma Theory (Academic, New York, 1972).

7. T.H. Dupree, Phys. Fluids **9**, 1773 (1966).

8. D. Montgomery, Phys. Rev. **123**, 1077 (1961).

9. I. Prigogine, C. George, F. Henin, L. Rosenfeld, Chemica Scripta **4**, 5 (1973).

10. I. Prigogine, C. George, F. Henin, Physica **45**, 418 (1969).

11. R. Balescu, Equilibrium and Nonequilibrium Statistical Mechanics, (Wiley-Interscience, New York, 1975).

12. R. Balescu, Statistical Mechanics of Charged Particles (Wiley-Interscience, New York, 1963).

13. C. George, Physica **65**, 277 (1973).

14. V. Škarka, C. George, Acad. R. Belgique, Bull. Cl. Sci. **69**, 210 (1983).

15. V. Škarka, C. George, Physica A **127**, 473 (1984).

16. N. van Kampen, Physica **23**, 641 (1957).

17. K. Case, Ann. Phys., NY **7**, 349 (1959).

18. V. Škarka, Physica A **156**, 651 (1989).

19. V. Škarka, P.V. Coveney, J. Phys. A: Math. Gen. **23**, 2439 (1990).

20. V. Škarka, P.V. Coveney, J. Phys. A: Math. Gen. **23**, 2463 (1990).

21. V. Škarka, Acad. R. Belgique, Bull. Cl. Sci. **64**, 578 (1978).

22. C. George, Acad. R. Belgique, Bull. Cl. Sci. **56**, 505 (1970).

23. V. Škarka, Physica A **133**, 442 (1985).

24. V. Škarka, Physica A **142**, 405 (1987).

25. Handbook of Mathematical Functions, edited by M. Abramowitz and I.A. Stegun (Dover Publications, New York 1970).

26. L.N.G. Filon, Proc. Roy. Soc. Edinburgh, **49**, 38 (1928).

27. B.S. Newberger, Comp. Phys. Com. **42**, 305 (1986).

28. S. Wolfram, Mathematica (Addison-Wesley Publishing, Redwood City, 1991).

Figure Captions

1. Elementary vertices.

2. All families of diagrams up to the first order in nonlinearity.

3. a and b. The local density excess corresponding to the sum of the linear and the nonlinear solution, analytical [Fig. 3a], and numerical [Fig. 3b], is plotted as a function of time (x-axis) and space (y-axis) for $u = 0.2$, $a = 0.3$, and $\lambda = 10$.

4. The superposition of the analytical and the numerical (lower amplitude) solutions of the linearized equation for $u = 0.2$, $a = 0.3$ and $\lambda = 100$.

5. The nonlinear part of the approximated and exact (larger amplitude) solutions plotted together for parameters of Fig. 4.

6. The total density excess [linear and nonlinear] for parameters of Figs. 4 and 5. Larger amplitude corresponds to the approximation.

7. Higherer amplitude corresponds to the total approximate solution for $u = 0.2$ and $\lambda = 100$, a different wave vector $a = 0.5$.

8. For $u = 0.2$, $a = 0.7$ and $\Lambda = 100$ the numerical solution has slightly higher amplitude.

9. The analytical results are of slightly lower amplitude for $u = 0.1$, $a = 0.3$ and $\lambda = 1000$.

10. Only the analytical solutions are available for $\lambda = 10000$ and $a = 0.3$.

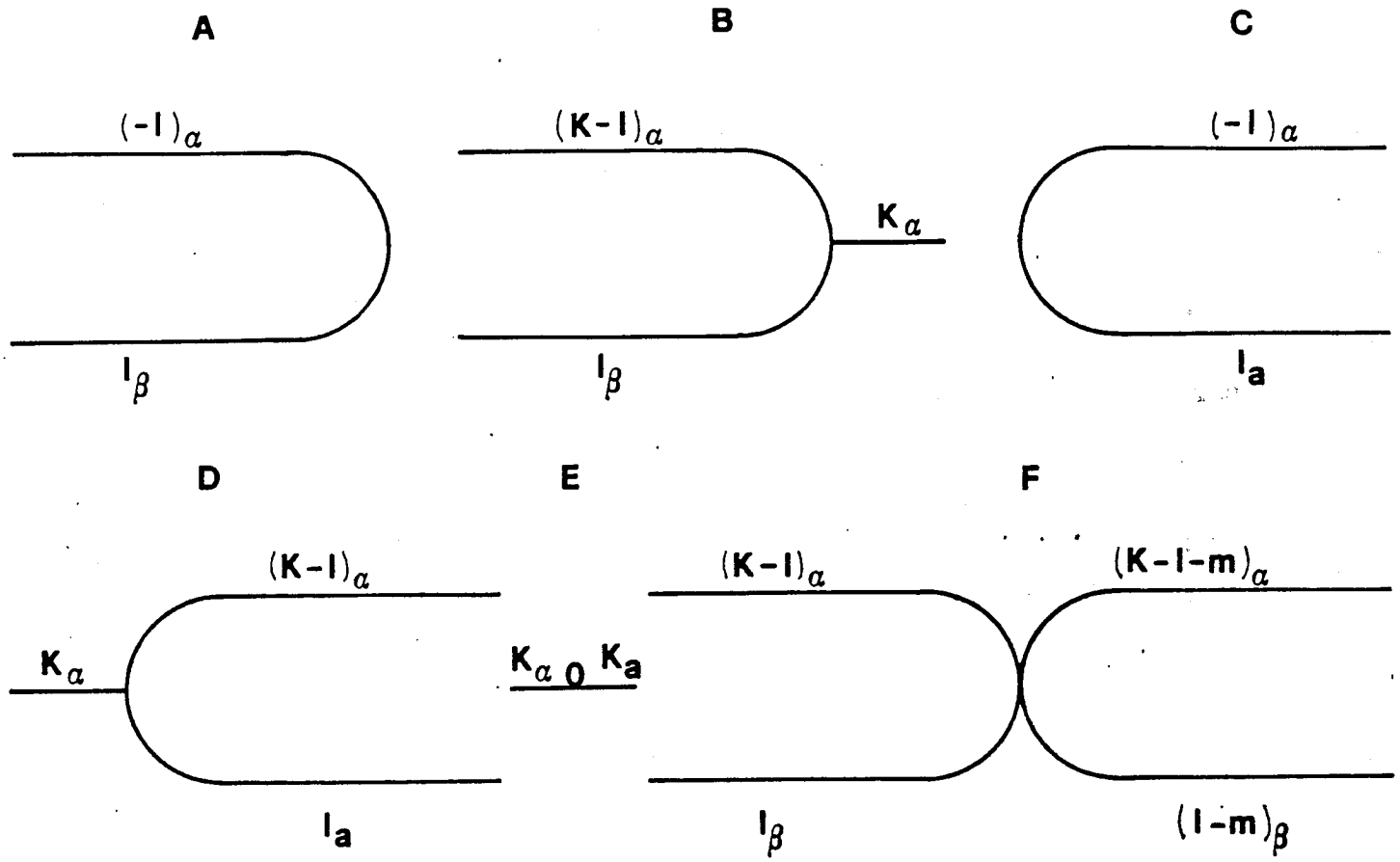
A
B
C
$(-l)_\alpha$
$(K-l)_\alpha$
K_α
$(-l)_\alpha$
l_β
l_β
l_a
D
E
F
$(K-l)_\alpha$
$(K-l)_\alpha$
$(K-l-m)_\alpha$
K_α
K_α 0 K_a
l_a
l_β
$(l-m)_\beta$

Fig.1

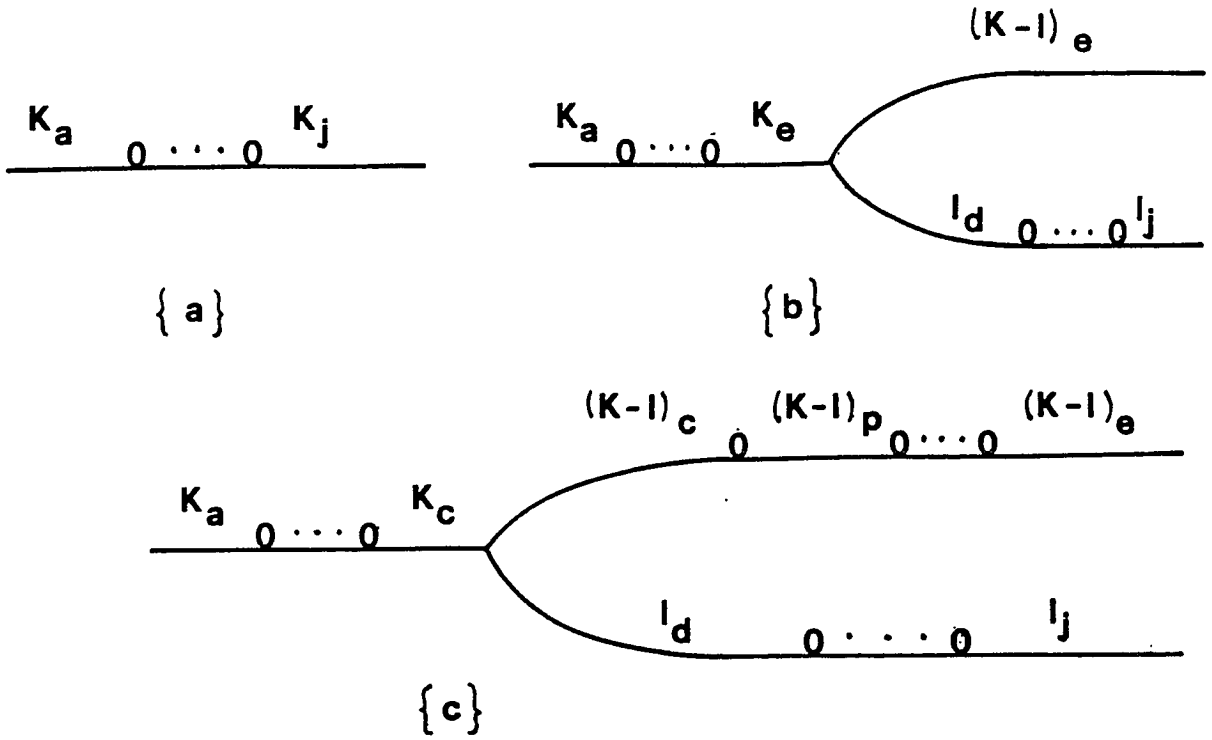

Fig.2

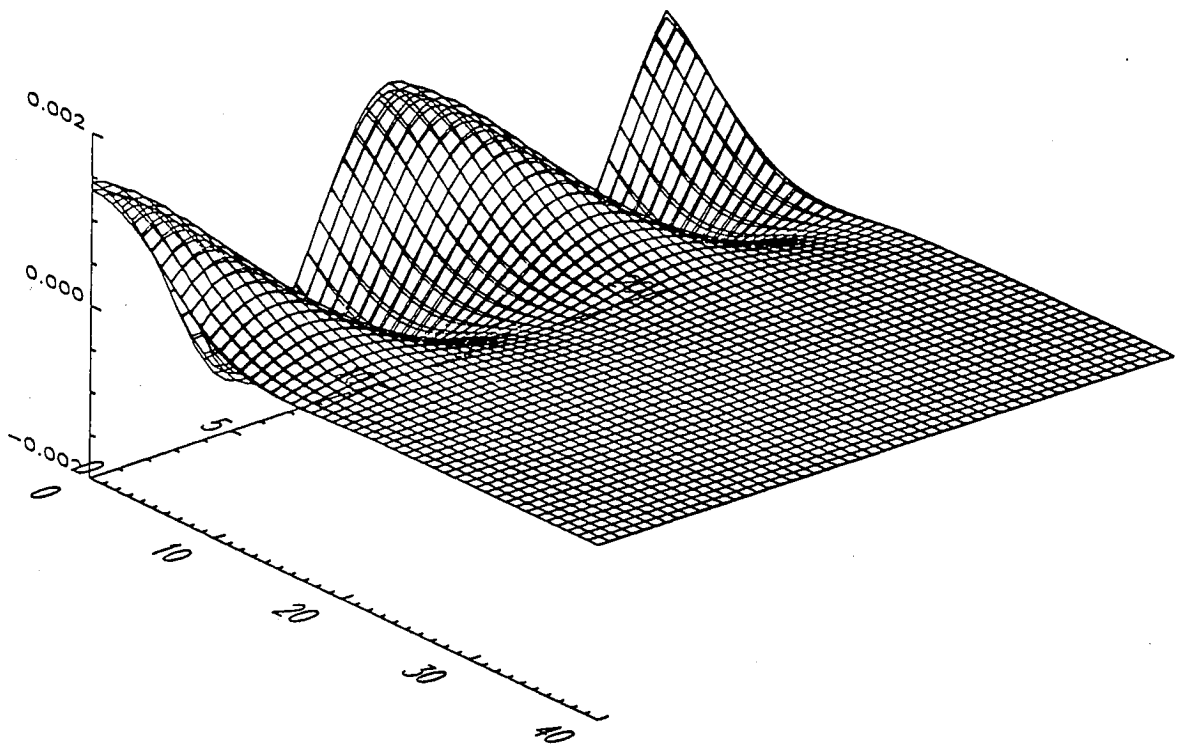

Fig. 3a

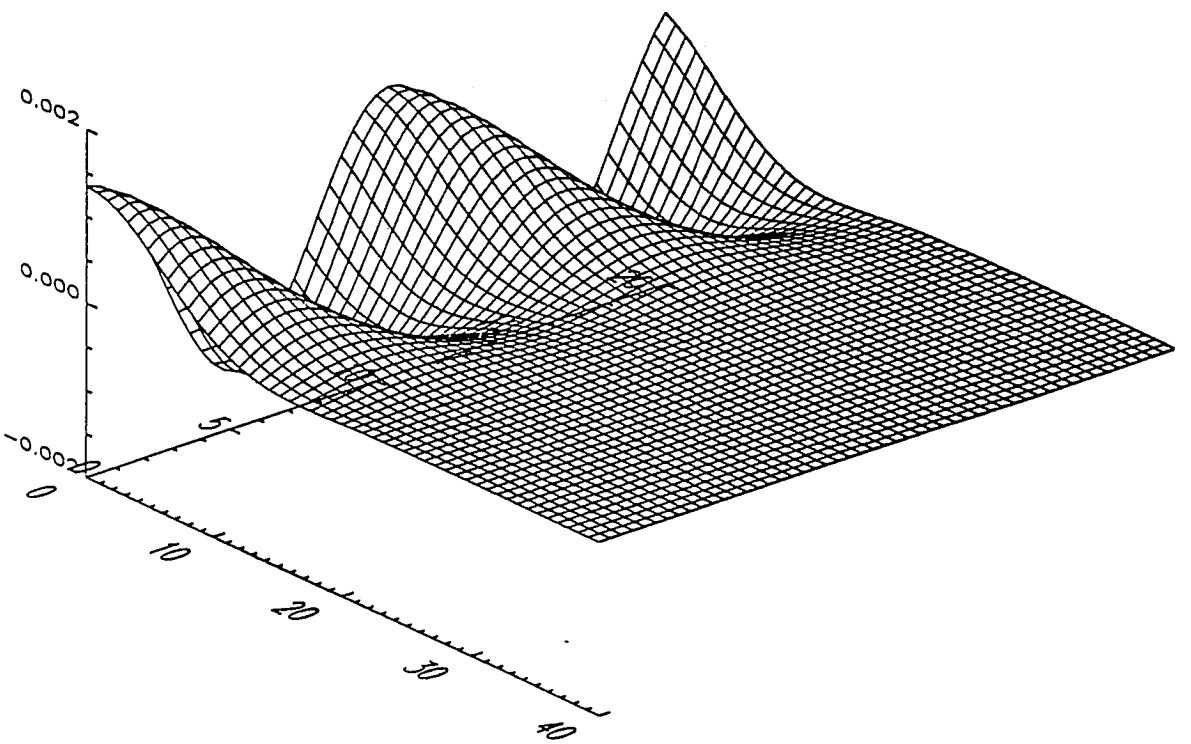

Fig. 3b

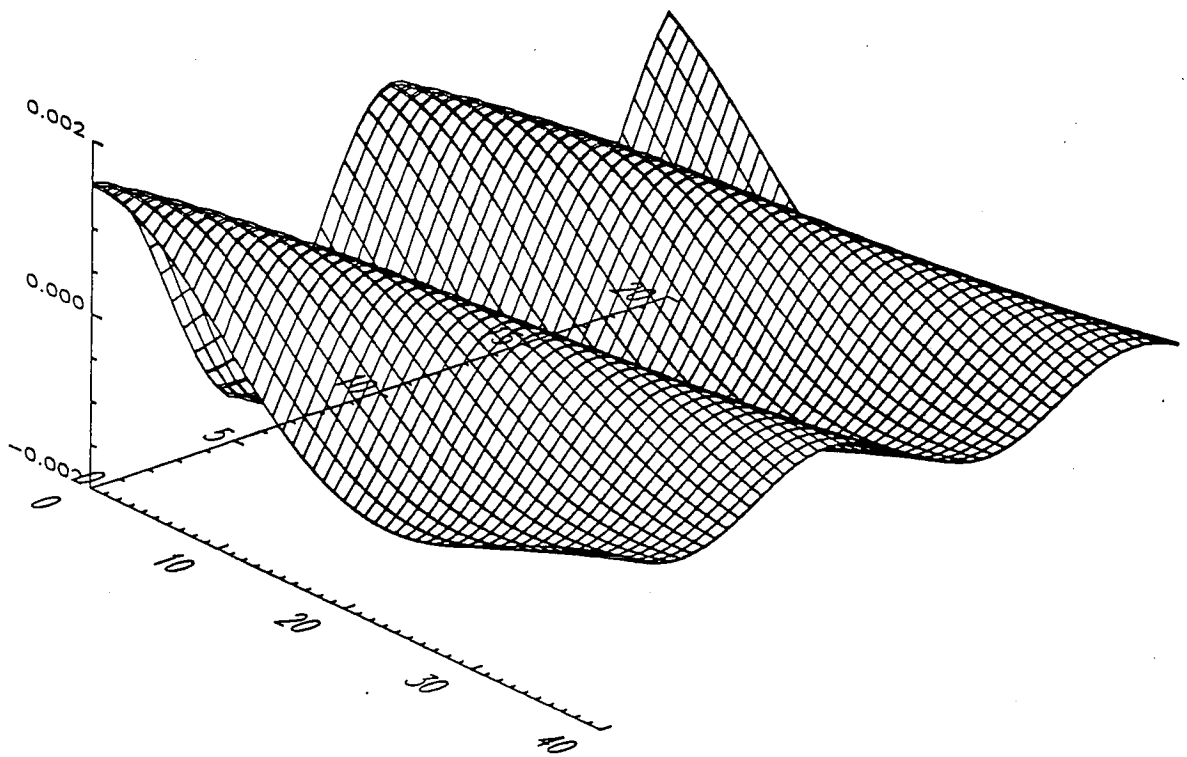

Fig. 4

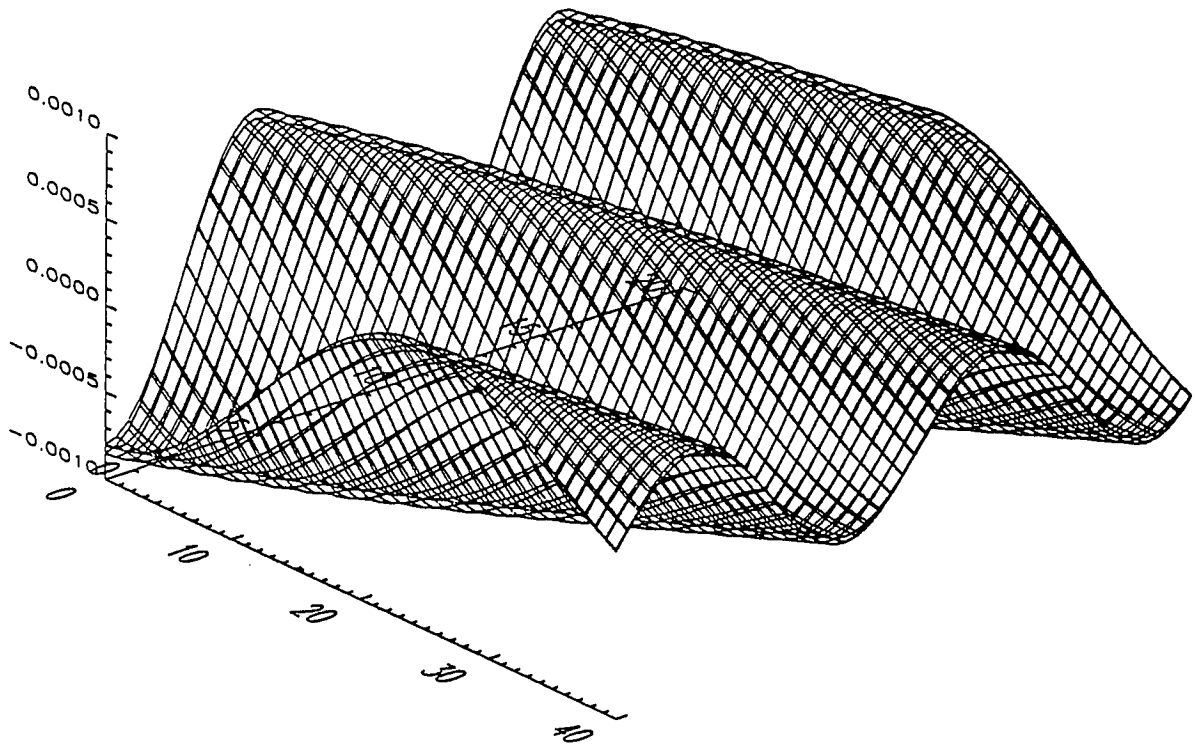

Fig. 5

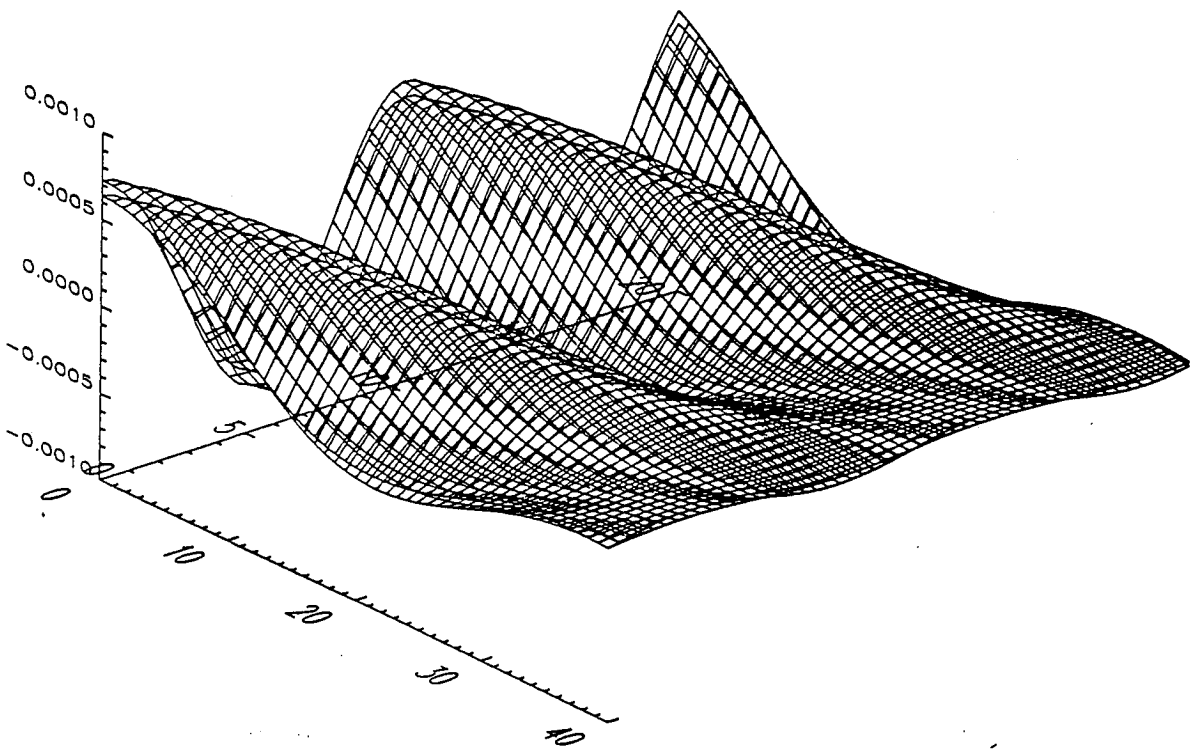

Fig. 6

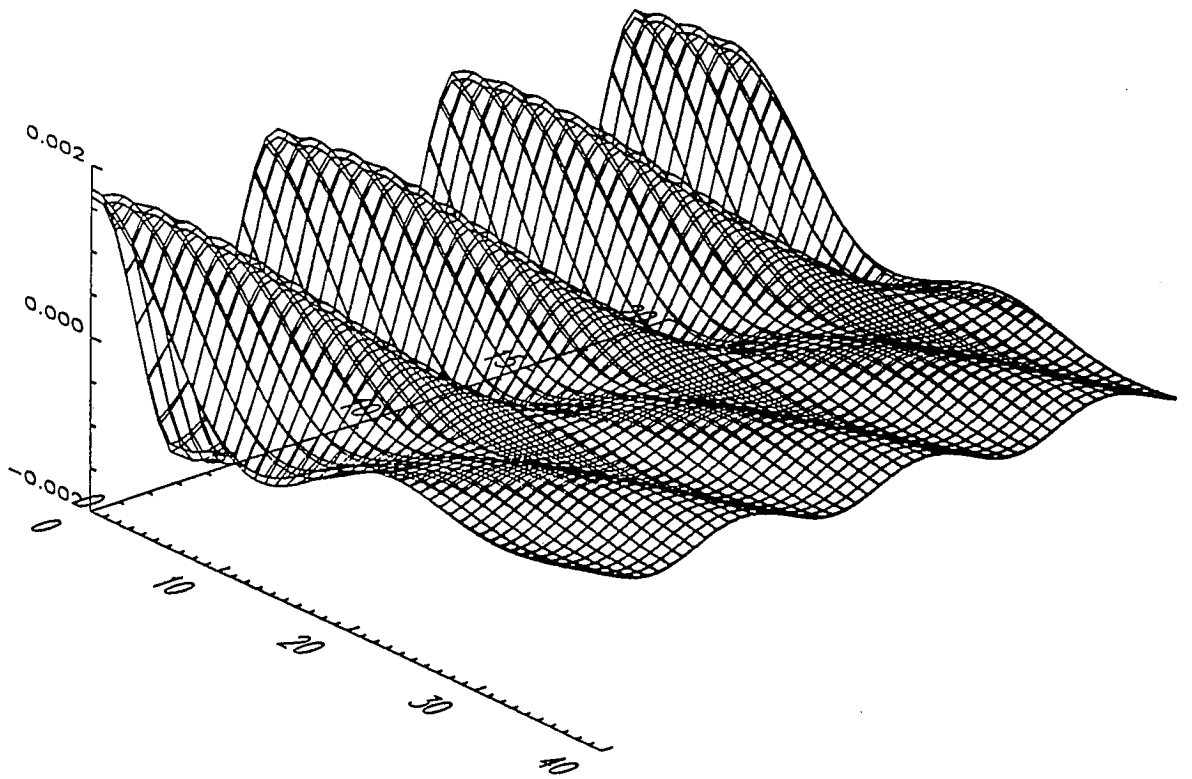

Fig. 7

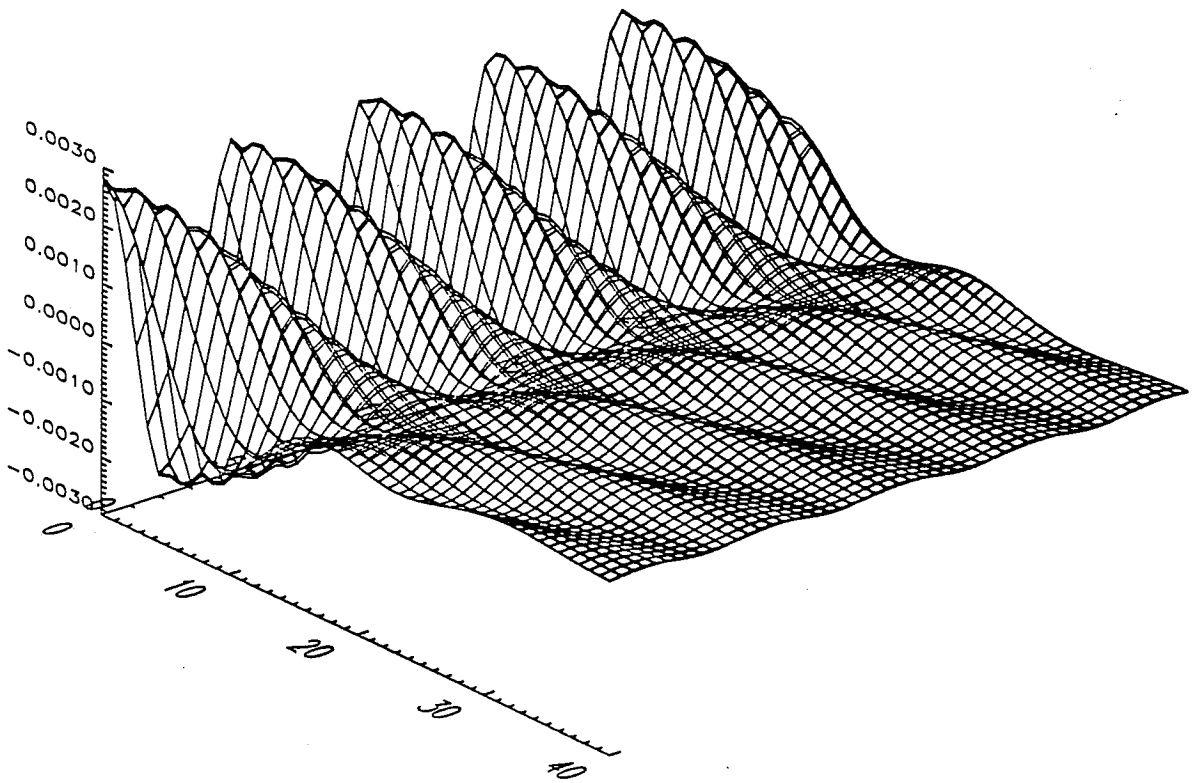

Fig. 8

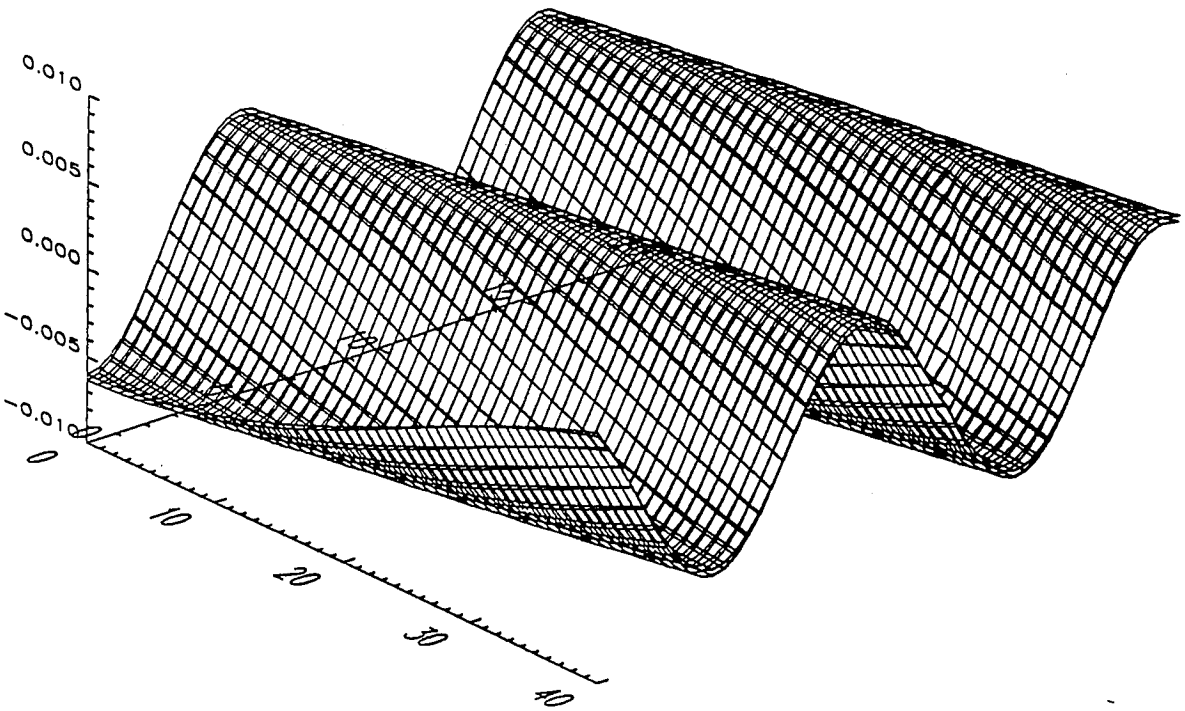

Fig. 9

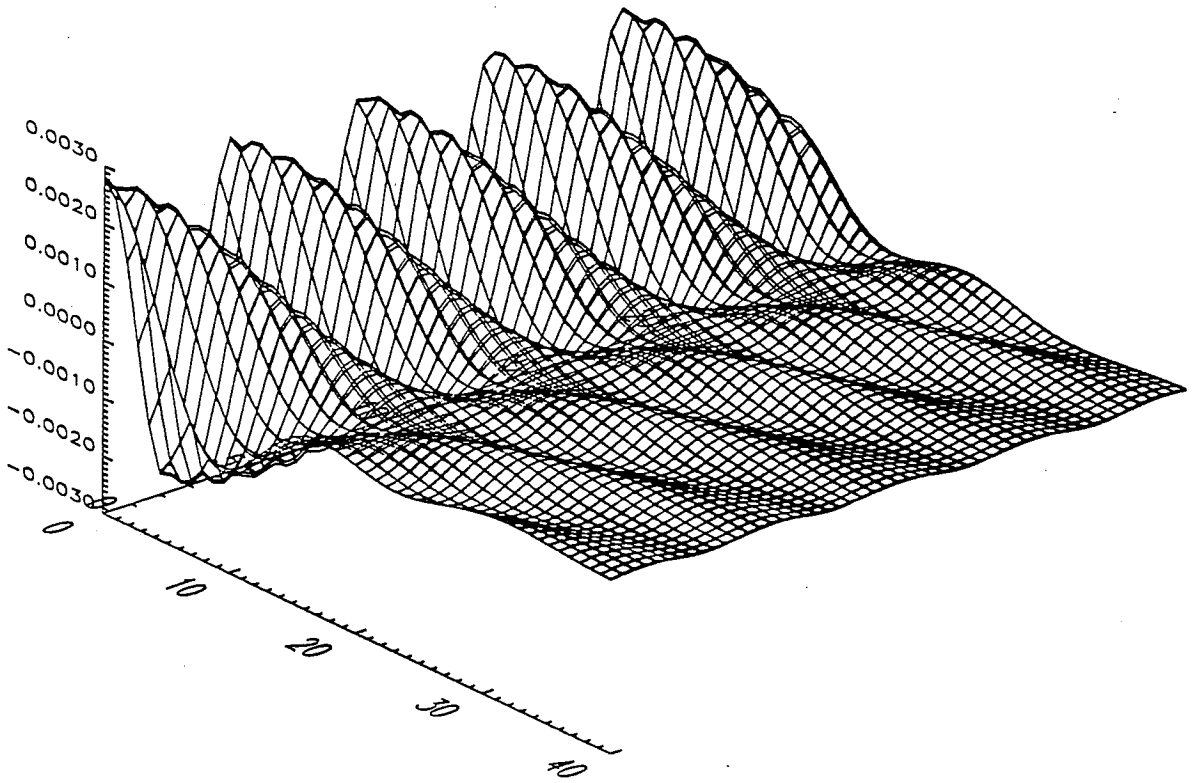

Fig. 8

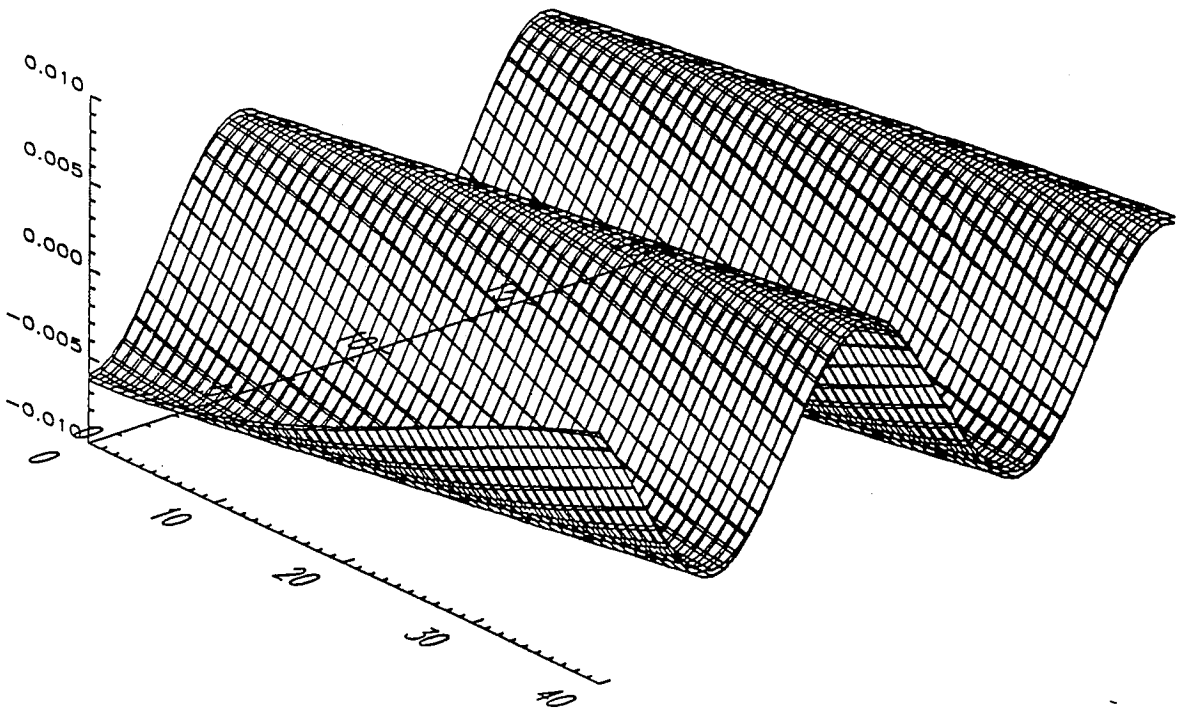

Fig. 9

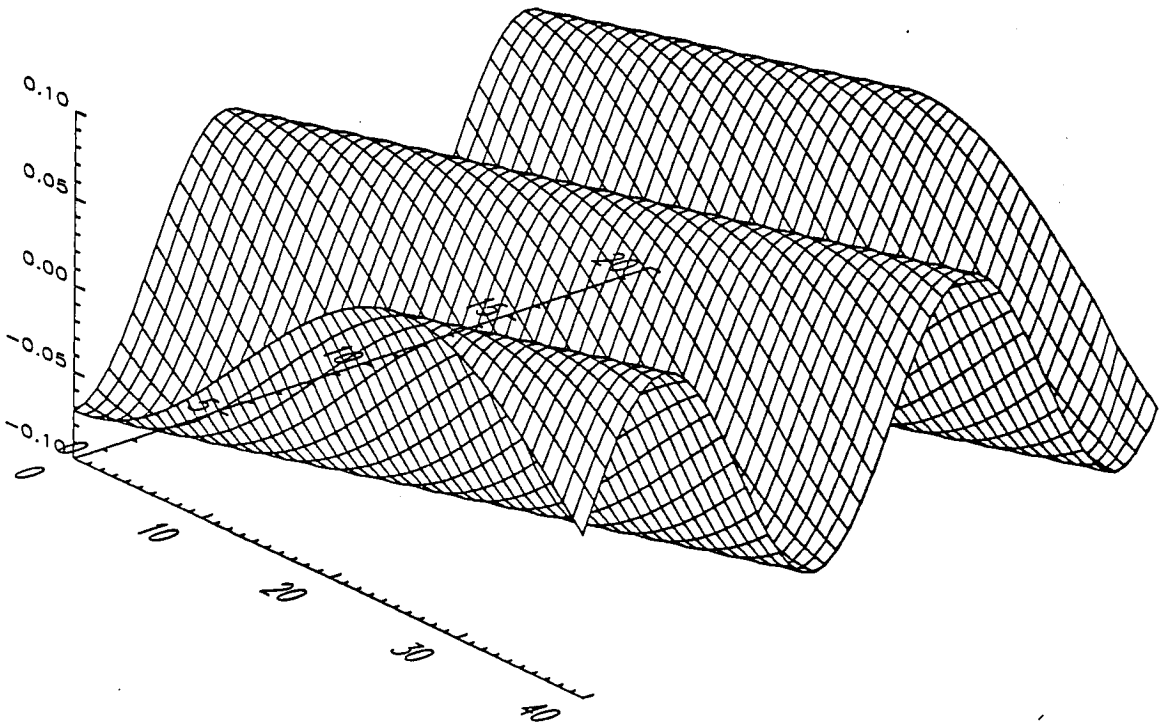

Fig. 10